ELSEVIER

Journal of Power Sources 81–82 (1999) 510–516

JOURNAL OF POWER SOURCES

www.elsevier.com/locate/jpowsour

A study on the effect of lithium insertion–extraction on the local structure of lithium manganese oxides using X-ray absorption spectroscopy

Oh-Sung Kwon [a], Min-Seuk Kim [b], Kwang-Bum Kim [a,*]

[a] *Department of Metallurgical Engineering, Yonsei University, 134 Shinchon-dong, Seodaemoon-gu, Seoul 120-749, South Korea*
[b] *Engineering Research Institute of Yonsei University, 134 Shinchon-dong, Seodaemoon-gu, Seoul 120-749, South Korea*

Abstract

Electronic and structural aspects of $Li_xMn_2O_4$ electrodes obtained from electrochemical oxidation–reduction process have been investigated by Mn K-edge X-ray absorption fine spectroscopy (XAFS). Charging of $Li_xMn_2O_4$ gave rise to an increase in the intensity of the peak at ca. 6543 eV and a shift of the overall peak positions towards higher energies in normalized X-ray absorption near-edge structure (XANES) spectra. Mean Mn–O bond length was at minimum in the charged state and it increased progressively with lithium insertion. Moreover, the extended X-ray absorption fine structure (EXAFS) spectrum of a second-charged $Li_xMn_2O_4$ electrode was somewhat different from that of the first one partly due to some disorder rendering different site energy.

Keywords: Lithium manganese oxide; X-ray absorption fine structure; Manganese oxidation state

1. Introduction

Rechargeable Li ion cells with transition metal oxide positive-electrodes have been the subject of widespread study. Among the transition-metal oxide materials, spinel $Li_xMn_2O_4$ has received considerable attention as the most promising positive-electrode material because of its low cost, high operating voltage, and acceptable environmental characteristics [1,2]. It has, however, a drawback of excessive capacity fading on cycling. Cyclability may be closely related to structural variations evolved as lithium is inserted and extracted. Thus, the detailed elucidation of the structural variations is essential for developing $Li_xMn_2O_4$ with good cyclability and control of the structure and electrochemical behavior of the material has studied extensively [3,4]. A structural analysis would give the useful information for understanding the electrochemical behavior of $Li_xMn_2O_4$. X-ray diffraction (XRD) technique has been widely used for this purpose [5]. However, the technique does not give sufficient information because it only provides average structural information with long-range order. On the other hand, X-ray absorption spectroscopy (XAS) is suitable for obtaining the information of electronic state and local structure without long-range order. In spite of its merit, very few XAS studies have been done on the electronic state and local structure of the $Li_xMn_2O_4$ electrodes during the cycling. Shiraishi et al. [6] recently reported a XAFS analysis of $LiMn_2O_4$ during the charge/discharge process. They suggested that the large variation in the local structure around the Mn atom during the charge/discharge process may be responsible for the cyclic instability of the battery material. Since XAS is element specific, this permits investigation of the chemical environment of a constituent element in a composite material in electrochemical systems [7].

The purpose of this study is to probe the structural changes accompanying lithium extraction–insertion from/into the spinel $LiMn_2O_4$ by investigation of atomic environment, using XAS. Therefore, electronic and structural aspects of $LiMn_2O_4$ electrode as a function of its state of charge have been investigated by Mn K-edge X-ray absorption fine spectroscopy (XAFS), which allows quantitative description of short-range order in structural

* Corresponding author. Tel.: +82-2-361-2839; Fax: +82-2-312-5375; E-mail: kbkim@bubble.yonsei.ac.kr

0378-7753/99/$ - see front matter
PII: S0378-7753(99)00210-4

analysis. Structural information such as interatomic distances and coordination numbers was determined for nearby coordination shells from extended X-ray absorption fine structure (EXAFS) [8,9]. The structure of the pre-edge peaks and absorption edge regions in Mn K-edge X-ray absorption near-edge structure (XANES) for approximately 0.8-e^- charged and discharged electrode has been shown to be sensitive to the effective charge of the absorbing manganese ion and therefore is correlated with manganese oxidation state.

2. Experimental

2.1. Preparation of $LiMn_2O_4$

Samples of spinel $LiMn_2O_4$ were prepared by reacting Li_2CO_3 (Aldrich, 99.997%) and electrolytic prepared MnO_2 (EMD, International Common Sample No. 17, Mitsui, Japan) under air in an alumina crucible. The starting materials, Li_2CO_3 and MnO_2, were first mixed at a 1:2 Li:Mn molar ratio in an agate mortar in ethanol for 1 h and calcinated at 500°C for 5 h and fired at 850°C under air for 24 h. After cooling, the process was repeated to minimize unreacted impurities (mainly Mn_2O_3 and Li_2MnO_3). The $LiMn_2O_4$ products were examined with XRD in automated Rigaku X-ray diffractometer. Lattice parameters were calculated against internal silicon standard. Chemical analysis was completed by inductively coupled plasma atomic emission spectrometer (ICP–AES).

2.2. Electrochemical experiments

The electrochemical cells consisted of a working electrode, lithium-metal foils as both counter and reference electrode, and an electrolyte of 1 M $LiPF_6$ in a 1:1 (volume ratio) mixture of ethylene carbonate (EC)/dimethoxyethane (DME). The working electrode was prepared by spreading the mixture of 80% $LiMn_2O_4$, 12.5% Denka black (used as conductive material) and 7.5% PVDF–HFP (PVDF = polyvinylidene fluoride, HFP = hexafluoropropylene) copolymer (Kynar FLEX 2801, Elf-Atochem America) dissolved in 1-methyl-2-pyrrolidinone (NMP) onto Al foil. The prepared electrode was then put into vacuum oven to evaporate the solvent at 150°C for about 5 h. Typically, the electrodes contained 2–3 mg of $LiMn_2O_4$. All electrochemical experiments were carried out in a three-electrode glass cell set up in an Ar-filled glove box (Mecaplex, Switzerland).

Electrochemical cells were cycled between 3.5 and 4.35 V vs. Li/Li^+ at a constant charging/discharging rate of $C/2$ using Solartron SI 1287. In the galvanostatic mode, the changes in Li content (Δx) was calculated from the elapsed time, the current and the mass of the active material in the cathode under the assumption that all the current passed was due to lithium insertion or extraction. After a certain concentration was reached, the cell was disassembled and the cathode dried in vacuum before performing XRD measurements.

2.3. X-ray diffraction measurements

Phase purity of the $LiMn_2O_4$ powders was examined with XRD in automated Rigaku X-ray diffractometer with Cu–K α radiation. The instrument was operated at 30 kV and 15 mA with a scanning rate 2°/min and a step size of 0.05°. In the case of delithiated and lithiated samples prepared by electrochemical routes they were dried in vacuum, then wrapped with polyethylene film for isolation from air, and exposed to air just before ex situ XRD measurements. In all cases the XRD patterns could be indexed on the basis of a cubic cell. The samples for EXAFS measurements also prepared in the same manner used for XRD.

2.4. X-ray absorption measurements

EXAFS measurements were performed above Mn K-edge at beamline 3Cl of Pohang Light Source (PLS). The storage ring was operated with electron energy of 2 GeV and a current between 80 and 120 mA. In all cases, double crystal monochromator Si (111) was used. All spectra were recorded in the transmission mode using ionization chambers filled with nitrogen. Calibration was carried out prior to all measurements using the first inflection point of the spectrum of Mn foil, i.e., Mn K-edge = 6539 eV, as a reference. The monochromator was scanned in the range from −200 to −20 eV, −20 to 25 eV with respect to Mn K-edge in increments of 5 and 0.3 eV, respectively, and in steps of 0.05 $Å^{-1}$ in the extended EXAFS region up to 7520 eV. The analysis of the EXAFS data was performed using UWXAFS 3.0 program package, which uses EXAFS ab initio modeling FEFF program [10,11].

3. Results and discussion

3.1. X-ray diffraction study and chemical analysis

The XRD patterns of reaction products obtained from EMD and Li_2CO_3 heat-treated under air for 24 h at 850°C are presented in Fig. 1. Single spinel-phase $LiMn_2O_4$ products were obtained and crystal structure was indexed to a cubic system with a lattice parameter a_0 of 8.24 Å, which is refined with a space group *Fd3m* (Oh^7) [12]. Chemical composition of the resulting compound was determined as $LiMn_2O_4$ (Li% and Mn% are 4.44 and 69.10%, respectively) by ICP–AES.

3.2. Charge / discharge curves

Typical charge/discharge behaviors of $Li/LiMn_2O_4$ cell at a constant current rate of $C/2$ are shown in Fig. 2.

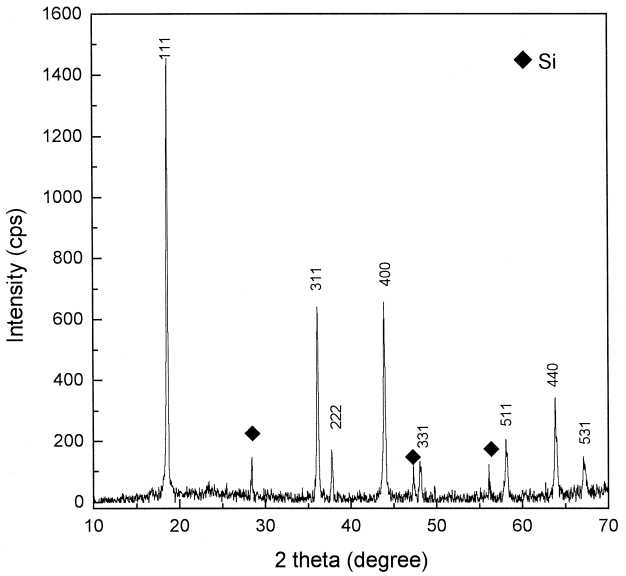

Fig. 1. Powder XRD pattern of the reaction product of EMD and Li_2CO_3 heated for 24 h at 850°C.

The cells were first charged from their rest voltage to 4.35 V vs. Li. The removal of approximately 0.8–9 Li^+ from the structure occurs in two steps. Two pairs of redox peaks in the 4 V region correspond to lithium ion extraction–insertion in tetrahedral site [4]. Two peaks corresponding to the reversible two step process for extracting Li from spinel $LiMn_2O_4$ are observed at the voltages of 4.02 and 4.15 V vs. Li/Li^+, respectively. During the initial cycle, the capacity loss mainly occurs at the higher voltage plateau, which may be due to the unstable two-phases coexisting during Li ion insertion–extraction into/from the spinel structure in Fig. 2.

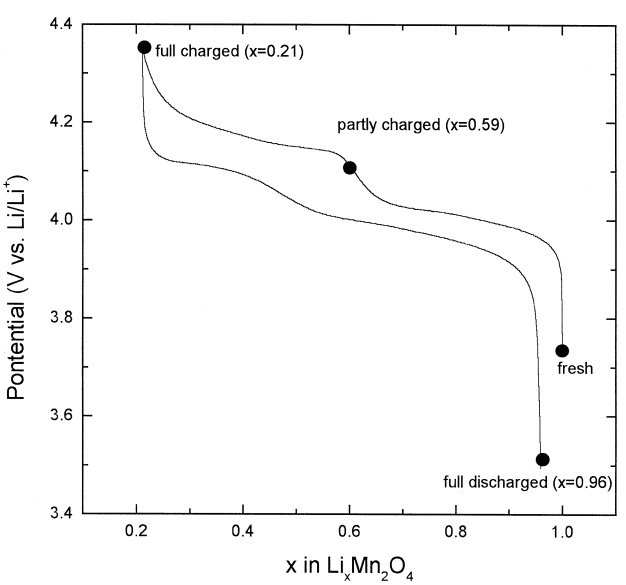

Fig. 2. Typical first charge/discharge behavior for $Li/LiMn_2O_4$ cell at a constant current rate of $C/2$. Cutoff: 3.5–4.35 V.

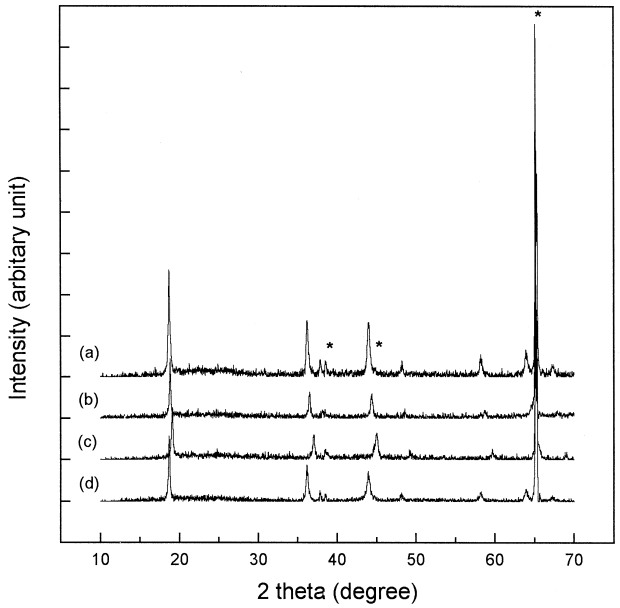

Fig. 3. XRD patterns of (a) fresh $LiMn_2O_4$, (b) partly charged ($Li_{0.59}Mn_2O_4$), (c) fully charged ($Li_{0.21}Mn_2O_4$), (d) fully discharged ($Li_{0.96}Mn_2O_4$). Peaks marked * arise from the aluminium foil current collector.

Ex situ XRD measurements were performed on samples that had been electrochemically inserted/extracted to different lithium concentrations. From the X-ray patterns in Fig. 3, it can be seen that spinel $LiMn_2O_4$ undergoes a phase transformation to $Li_{0.21}Mn_2O_4$. This transformation results in a shift of all of the observed spinel peaks towards higher angles as lithium is removed from the spinel structure. The $Li_xMn_2O_4$ sample has values of a_0 for $x = 0.59$, $x = 0.21$, and $x = 0.96$ equal to 8.16, 8.05, and 8.24 Å.

3.3. EXAFS analysis

Background below the edge jump was subtracted by a linear fit through the pre-edge region and extrapolation

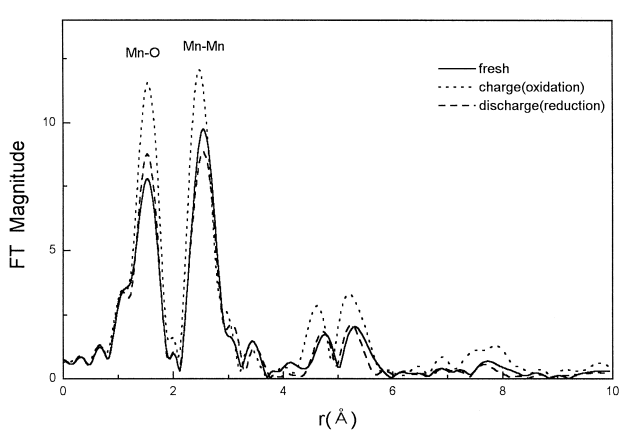

Fig. 4. Fourier transformed EXAFS spectra of composite $LiMn_2O_4$ obtained from charge/discharge process.

Table 1
Structural parameters for spinel lithium manganese oxides obtained using single-scattering contributions to the EXAFS up to 3.6 Å[a]. They are obtained by nonlinear least squares curve fits to ab initio calculated data using FEFF6.01

	Mn–O		Mn–Mn	
	Bond length (Å)	σ^2	Bond length (Å)	σ^2
Fresh	1.923	0.00535	2.908	0.00707
First charge	1.907	0.00405	2.839	0.00678
First discharge	1.920	0.00508	2.900	0.00892
Second charge	1.907	0.00510	2.854	0.00784

[a] Numbers of N are fixed to six in both Mn–O and Mn–Mn shell.

through the EXAFS region. Background above the EXAFS region was determined by fitting a cubic spline and optimized according to the criteria described by Cook and Sayers [13]. The spectra were normalized by dividing the X-ray absorption by the height of the spectrum at around 50 eV above the edge [14]. Normalized EXAFS were converted from energy to k and weighted by k^3 to compensate for attenuation of the amplitude in the EXAFS spectra at high k. All prominent shells in the resulting radial distribution function were back-Fourier transformed collectively using a window of 1.0 to 3.6 Å. Ab initio XAS code FEFF6.01 using the atomic coordinates of spinel lithium manganese oxides was used for fitting the filtered EXAFS functions. The coordination number for the first shell of oxygen atoms was fixed to the crystallographic value of six for all the samples. In the case of the second coordination shell, consisting of manganese atoms in neighboring 16d octahedral sites, the coordination number was also fixed to six. In all cases the agreement between experimental and theoretical curves over the k range of 3–12 $Å^{-1}$ gave statistical residues of less than 0.02.

Fig. 4 shows Fourier transformed Mn K-edge EXAFS spectra of the products obtained from electrochemical oxidation–reduction process. The amplitudes of Mn–O and Mn–Mn shells increase as the material is charged. The essential structural information can be obtained from the data in the first two intense peaks in the Fourier transform, due to the highly stable symmetry of spinel structure. The first coordination shell is related to the oxygen octahedra. The second coordination shell is related to the first cationic neighbors (Mn). The Mn–O distances, Mn–Mn distances, and the Debye–Waller factor σ^2 for the two single-scattering paths from the curve-fitting refinement are given in Table 1. Interatomic distances determined from the EXAFS show contraction of the Mn–O distance from 1.92 to 1.90 Å, and of Mn–Mn distances from 2.90 to 2.84 Å after lithium extraction from $LiMn_2O_4$ composite elec-

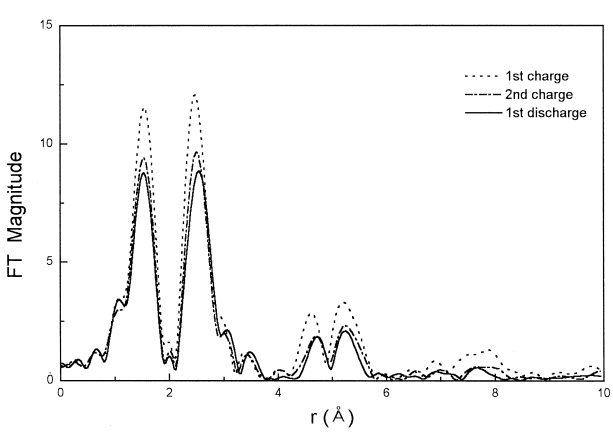

Fig. 5. Fourier transformed EXAFS spectra of composite $LiMn_2O_4$. First charge (dot), first discharge (solid), second charge (dash–dot).

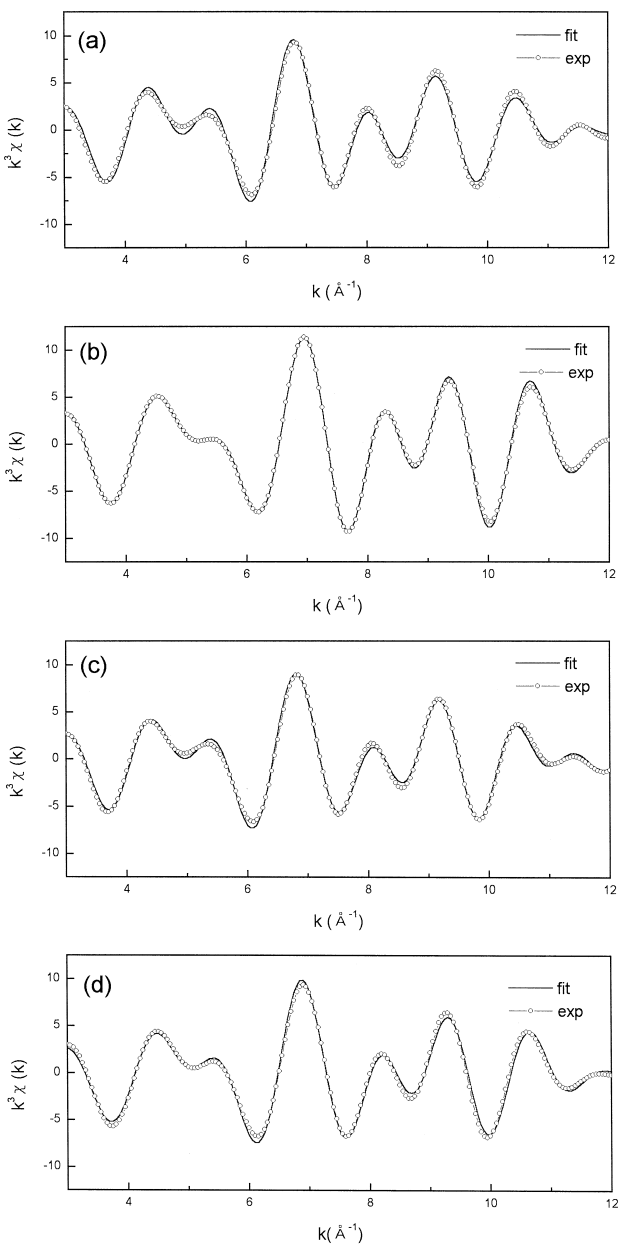

Fig. 6. Mn K-edge EXAFS spectra in k-space of (a) the fresh, (b) the first charge, (c) the first discharge, (d) the second charge.

trode. The data also show a small decrease in the Debye–Waller factors when lithium is extracted electrochemically, which may be attributed to removal of a static distribution of interatomic distances when a mixed $Mn^{3+}/^{4+}$ composite electrode is oxidized during charging process. Reinsertion of lithium into $Li_{0.21}Mn_2O_4$ results in almost complete restoration of the spectrum of the fresh $LiMn_2O_4$ composite electrode in the view of position of bond distances and intensity.

The Fourier transformed EXAFS spectra of the spinel materials according to cycling are shown in Fig. 5. Plots of $k^3\ \chi(k)$ vs. k for the Fourier transformed EXAFS spectra shown in Figs. 4 and 5 are also given in Fig. 6. A general intensity attenuation of the signals is observed in the second-charged material compared to the first one. In addition, only a small increase of the Debye–Waller factor is recorded, indicative of some small disorder in the second-charged material. This phenomenon may be a clue to the capacity loss occurred mainly at a higher voltage plateau of the charge curves in Fig. 2. The cycled spinel material may be somewhat different from the one before, partly due to some disorder rendering different site energy. Further studies are expected to obtain insight into the phenomenon.

3.4. XANES analysis

The XANES spectra of the spinel manganese oxide samples were characterized by the features labeled A to D shown for the experimental spectra of spinel $LiMn_2O_4$ electrodes as a function of their states of charge and discharge in Fig. 7. At the manganese pre-edge, the spectrum of MnO_2 is typical of manganese (IV) in an octahedral surrounding; the intensity of the pre-edge is strong and the top of the main edge is featureless.

3.4.1. Main edge

The main absorption edge rises in two distinct steps which may be distinguished as two inflection points B_1 and B_2. Two strong resonance C and D are shown just

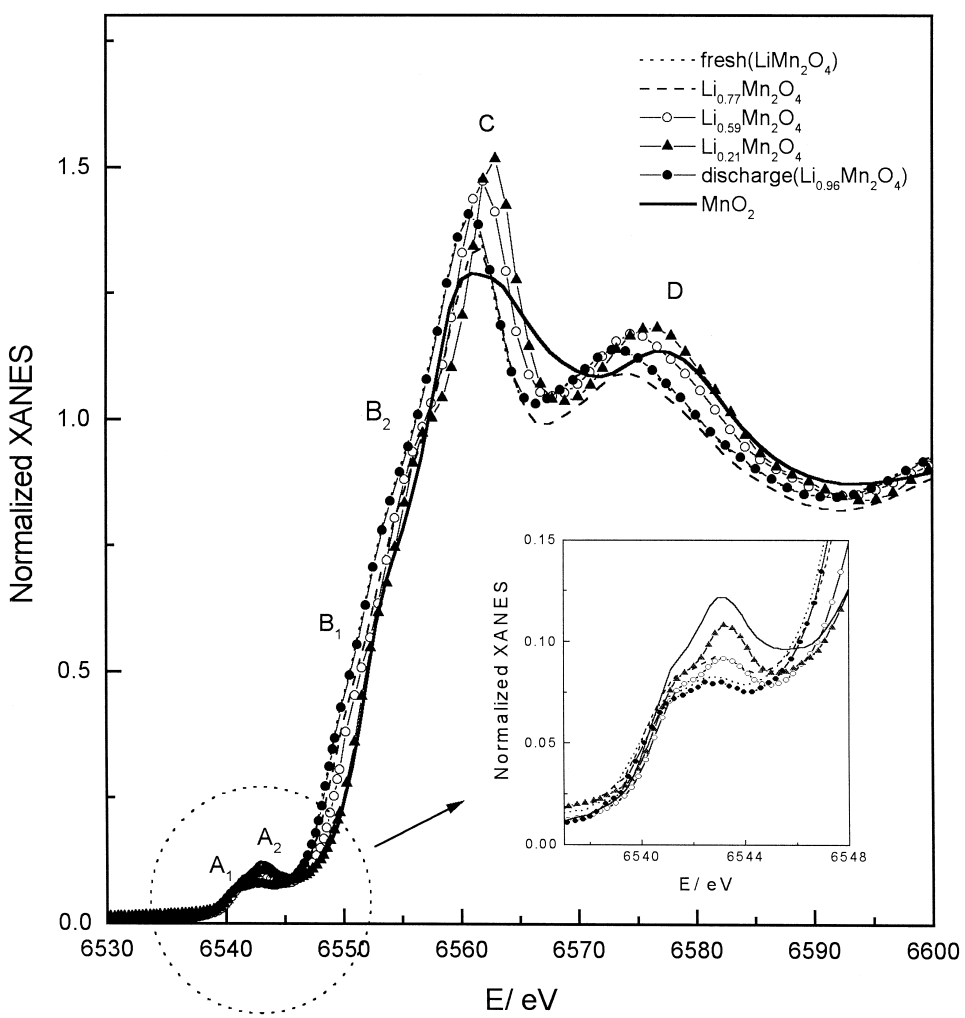

Fig. 7. Mn K-edge XANES spectra of composite $Li_xMn_2O_4$. The insert shows an expanded view of the region of the spectra containing the pre-edge feature.

above threshold, beyond which the spectra show EXAFS. The intense feature (C) centered about 6560 eV is expected to be composed of dipole-allowed transitions of the 1s electron to empty 4p orbital [15].

Systematic shifts of the pre-edge, the main edge and the edge peak positions are observed in the normalized XANES shown in Fig. 7. The shifts are quantitatively characterized in the second derivative XANES shown in Fig. 8. As Li^+ is extracted from the spinel $LiMn_2O_4$ electrode by charging, the energies of the pre-edge and main edge absorption increase with increasing oxidation state. The energy at which an absorption edge occurs is characteristic of the absorbing manganese atom. The loss of an electron by oxidation causes the remaining electrons to be bound more tightly by the nucleus [16]. Therefore, the greater X-ray energy is required to remove the remaining electrons. The shoulders B_1, B_2 and strong resonance C are strongly affected by 0.8 mol Li^+ extraction from $LiMn_2O_4$, changing broad features to sharply defined shoulders and an overall displacement of their second derivative peaks by 2–3 eV to higher energy in Fig. 9. Reinsertion of lithium into $Li_{0.21}Mn_2O_4$ results in almost complete restoration of the spectrum of the fresh $LiMn_2O_4$ electrode, including the position of edge and re-broadening of the main edge structure and resonance C and D. The main edge features appear to be shifted consistent with the change in both bond lengths (Mn–O) and manganese oxidation state.

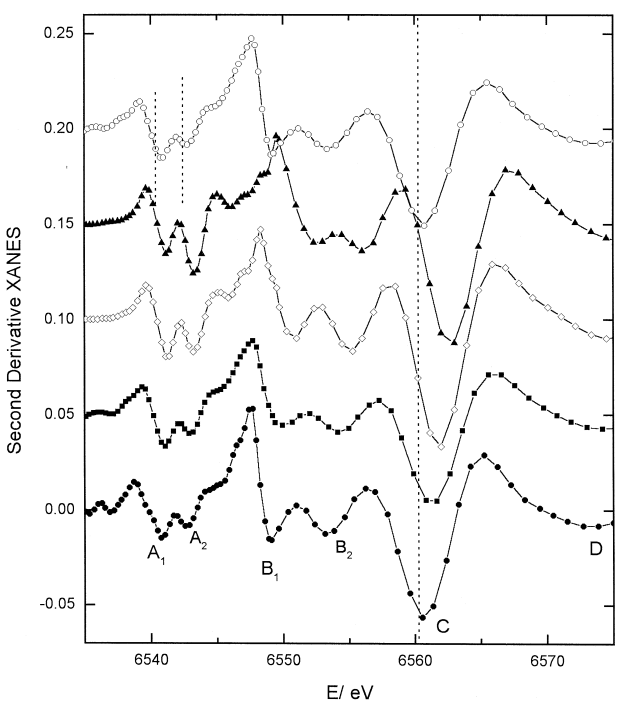

Fig. 8. Mn K-edge second derivative XANES spectra of composite $Li_xMn_2O_4$. Fresh ($x = 1$, close circle), $x = 0.77$ (close square), $x = 0.59$ (open diamond), fully charged ($x = 0.21$, close up triangle), fully discharged ($x = 0.96$, open circle).

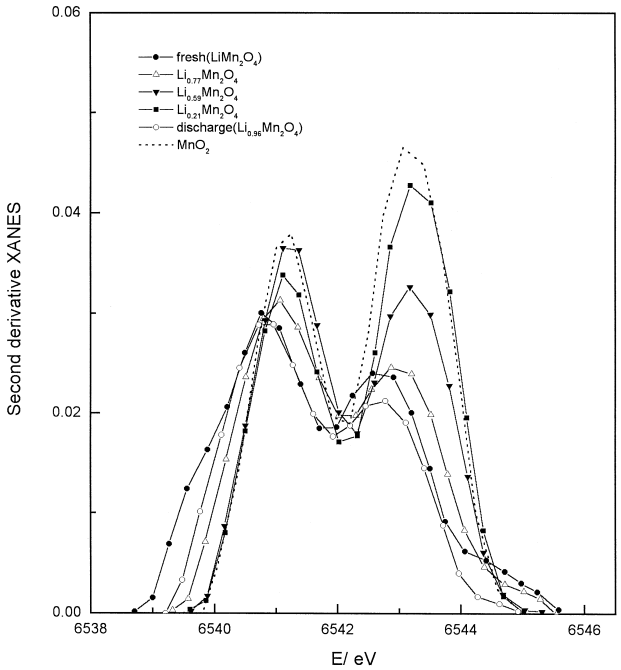

Fig. 9. Pre-edge region of Mn K-edge second derivative XANES spectra for $Li_xMn_2O_4$ after background substraction.

3.4.2. Pre-edge

Among these edge features, the pre-edge is of principal interest here because its position is related to the average oxidation state of the spectrum. Although the 1s-to-3d transition is formally dipole forbidden in octahedral coordination, the weak intensities of the A_1 and A_2 peaks near 6540 eV are shown in absorption due to direct quadrupole transition or to the mixing of 3d and 4p orbital in the local structure, conferring some dipole-allowed character [15,17].

For the pre-edge peak analysis, the energy of the pre-edge peak was defined to be the centroid of a Gaussian fit to the peak after the background subtraction of second derivatives of the Mn K-edge XANES spectra [16]. In Fig. 9, there is a change in intensity and shape of the pre-edge peaks that depend only on the change in lithium content. One possibility is that an increase in pre-edge peak (A_2) intensity (from fresh $LiMn_2O_4$ to full charged $Li_{0.21}Mn_2O_4$) correlates with increase in the Mn^{4+}/Mn^{3+} ratio [17]. As was shown in Fig. 9, the energy position and shape of peaks (A_1, A_2) in charged sample are similar to those of MnO_2 (Mn^{4+}). A second possibility might explain the feature in pre-edge in terms of changes in average Mn–O bond distances, which is clarified by curve fitting with ab initio modeling FEFF6.01. This result is in accordance with the fact that Mean Mn–O bond length is at minimum in charged state and increases progressively with lithium reinsertion (reduction) in EXAFS analysis. On the other hand, the small magnitude of these features for both the charged state and the discharged state is indicative of an octahedral environment with only slight distortion.

The pre-edge spectra of the fresh $LiMn_2O_4$ electrode and the lithium-reinserted electrode are very similar to each other with identical energies of the two samples.

4. Conclusions

Single spinel-phase $LiMn_2O_4$ were obtained by solid state reaction. The products formed from electrochemical oxidation–reduction process with the $LiMn_2O_4$ were investigated by XAS. It was found that charging of $LiMn_2O_4$ gave rise to an increase in the intensity of the peak at ca. 6543 eV in the pre-edge features and a shift of the overall peak positions in the main edge features towards higher energies. EXAFS analysis showed that mean Mn–O bond length was at minimum in the charged state of the spinel material and that it increased progressively with lithium insertion. A general attenuation in intensity of the signals was observed in a second-charged material compared to the first one. In addition, a small increase of the Debye–Waller factor was recorded, indicative of some disorder in the second-charged material.

Acknowledgements

This study was supported by Korea Science and Engineering Foundation (No. 96-0300-17-01-03). Experiments at PLS were supported in part by MOST and POSCO.

References

[1] J.M. Tarascon, D. Guyomard, J. Electrochem. Soc. 138 (1991) 2864.
[2] V. Manev, B. Banov, A. Monchilov, A. Nassalevska, J. Power Sources 57 (1995) 99.
[3] T. Ohzuku, M. Kitagawa, T. Hirai, J. Electrochem. Soc. 137 (1990) 769.
[4] Y. Xia, M. Yoshio, J. Electrochem. Soc. 143 (1996) 825.
[5] M.N. Richard, I. Koetschan, J.R. Dahn, J. Electrochem. Soc. 144 (1997) 554.
[6] Y. Shiraishi, I. Nakai, T. Tsubata, T. Himeda, F. Nishikawa, J. Solid State Chem. 133 (1997) 587.
[7] M.F. Toney, J. McBreen, The Electrochemical Society Interface 2 (1993) 22.
[8] D.C. Koningsberger, R. Prins (Eds.), X-ray Absorption: Principles, Application, Techniques of EXAFS, SEXAFS and XANES, Wiley, New York, 1988.
[9] B. Teo, EXAFS: Basic Principles and Data Analysis, Springer, New York, 1986.
[10] J.J. Rehr, S.I. Zabinsky, R.C. Albers, Phys. Rev. Lett. 69 (1992) 3397.
[11] P.A. O'Day, J.J. Rehr, S.I. Zabinsky, G.E. Brown Jr., J. Am. Chem. Soc. 116 (1994) 2938.
[12] C.J. Chen, M. Greenblatt, J.V. Waszczak, Mater. Res. Bull. 21 (1986) 609.
[13] J.W. Cook Jr., D.E. Sayers, J. Appl. Phys. 52 (1981) 5024.
[14] Y. Iwasawa, X-ray Absorption Fine Structure for Catalysts and Surface, Chap. 8, World Sci., Singapore, 1996.
[15] I.J. Pickering, G.N. George, J.T. Lewandowski, A.J. Jacobson, J. Am. Chem. Soc. 115 (1993) 4137.
[16] S. Bajt, S.R. Sutton, J.S. Delaney, Geochimica et Cosmochimica Acta 58 (1994) 5209.
[17] A. Manceau, A.I. Corshkov, V.A. Drits, American Mineralogist 77 (1992) 1133.